

# Electrochemistry of Copper in Polyacrylic Acid: The Electrode Mechanism and Analytical Application for Gaseous Hydrogen Peroxide Detection

Leon Stojanov, Angela Rafailovska, Vasko Jovanovski, and Valentin Mirceski\*



Cite This: <https://doi.org/10.1021/acs.jpcc.2c05259>



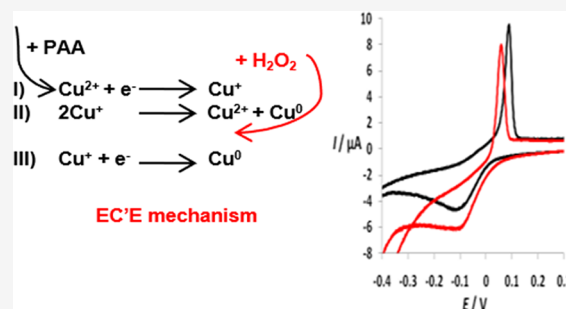
Read Online

ACCESS |

Metrics & More

Article Recommendations

**ABSTRACT:** Electrode reaction of copper(II) reduction in an aqueous solution of polyacrylic acid (PAA) is studied by means of cyclic staircase and square-wave voltammetry to establish a basis for an electrochemical sensor for gaseous hydrogen peroxide detection. It has been determined that the reduction mechanism at a glassy carbon electrode follows a two-step, consecutive electron transfer reaction scheme of  $\text{Cu}^{2+}$  to the final copper solid deposit, via the formation of the intermediate  $\text{Cu}^+$  ions, which are subject to a fast disproportionation reaction. Experimental data have been supported by theoretical considerations and simulations based on EC'E electrode mechanism, where E designates an electrode reaction, whereas C' is a homogeneous regenerative chemical reaction. Estimated thermodynamic and kinetic data of the electrode mechanism suggest stabilization of the intermediate  $\text{Cu}^+$  form by PAA in comparison with a pure aqueous medium. Commercially available screen-printed carbon electrodes were covered with a film of 1% (mass percent) of aqueous PAA solution containing  $\text{Cu}^{2+}$  ions, which proves to be a promising platform for gaseous  $\text{H}_2\text{O}_2$  detection, where the  $\text{Cu}^{2+}/\text{Cu}^+$  couple serves as a redox mediator for  $\text{H}_2\text{O}_2$  reduction, with a limit of detection at a sub- $\mu\text{g dm}^{-3}$  concentration level in the gas phase.



## 1. INTRODUCTION

Polyacrylic acid (PAA) is a well-known polymer and a suitable polyelectrolyte with a broad range of applications,<sup>1–5</sup> which has attracted notable interest due to superior biocompatibility,<sup>6–10</sup> perfect water absorptivity, and good thin-film formability.<sup>11–14</sup> Particular properties of PAA depend strongly on the degree of cross-linking of the polymeric molecules, while significantly cross-linked PAA is water insoluble, the noncross-linked form is water soluble, and the gel phase can be formed under a broad range of pH values. The physicochemical properties of the PAA gel are predominantly controlled by the concentration and the size of polymeric molecules, temperature, ionic strength, the type of counter ions, etc. The noncross-linked PAA is partly dissociated in water, and the  $\text{pK}_a$  value is estimated to be close to 4,<sup>15,16</sup> the exact value depending on the polymer size (molar mass). The molecular size is also important for the pH-dependent conformational state in an aqueous solution. Commonly, polymeric molecules with a high molar mass ( $M > 16,000$  g/mol) change their conformation depending on pH.<sup>17</sup> Due to polyelectrolytic features and versatility of physicochemical characteristics, the aqueous PAA gel is an excellent basis for the preparation of electrochemical gas sensors.<sup>18–20</sup> The motivation of the current study is to use PAA as a medium for gaseous hydrogen peroxide ( $\text{H}_2\text{O}_2$ ) electrochemical

detection, using copper(II) ions as a redox mediator. Thus, the electrode mechanism of copper(II) reduction in a noncross-linked PAA aqueous solution at a glassy carbon electrode was studied in detail using cyclic staircase (CSV) and square-wave voltammetry (SWV). Detection of gaseous  $\text{H}_2\text{O}_2$  is important in various fields, as in medicine, where gaseous  $\text{H}_2\text{O}_2$  in the human breath is associated with a range of pathological conditions,<sup>21,22</sup> as well as in the environment protection related to occupational risk of numerous hydrogen peroxide-related industries.<sup>23</sup> More importantly, gaseous  $\text{H}_2\text{O}_2$  detection is a highly relevant subject for security issues, as most the homemade peroxo-explosives, which are frequently misused in terroristic attacks (e.g., triacetone triperoxide or diacetone diperoxide) can be detected through gaseous  $\text{H}_2\text{O}_2$ .<sup>24</sup>

On the other hand, the electrochemistry of copper species was exploited for the preparation of a variety of electrochemical sensors,<sup>25</sup> where copper was used either as an

Received: July 25, 2022

Revised: September 23, 2022

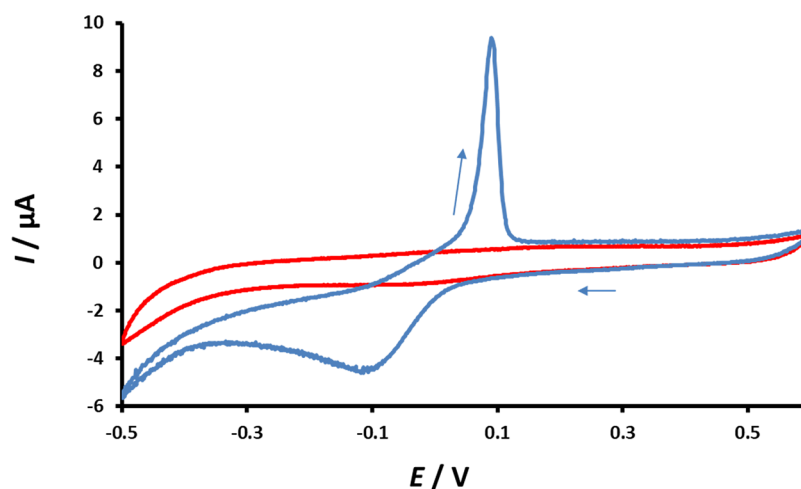
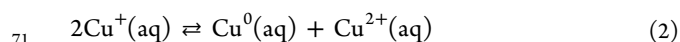
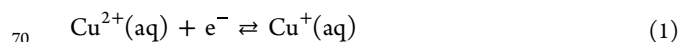
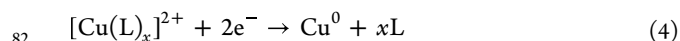


**Figure 1.** Typical cyclic staircase voltammogram of  $3 \times 10^{-4} \text{ mol L}^{-1} \text{ Cu}^{2+}$  ions (blue curve) in the supporting electrolyte containing 1% PAA and  $0.1 \text{ mol L}^{-1} \text{ KNO}_3$  with the step potential of  $\Delta E = 1 \text{ mV}$  and the scan rate of  $\nu = 10 \text{ mV/s}$  at a glassy carbon electrode. The red curve corresponds to the response of the supporting electrolyte in the absence of copper.

electrocatalyst (mostly in a form of copper nanoparticles),<sup>26,27</sup> or using copper ions as a redox mediator.<sup>28</sup> As is well known, electrochemical reduction of  $\text{Cu}^{2+}$  ions in a noncomplexing aqueous medium follows a two-step mechanism (eqs 1 and 3), proceeding via the formation of  $\text{Cu}^+$  ions as a labile intermediate, followed by a fast disproportionation reaction<sup>29,30</sup>



According to the Bockris–Mattson EE mechanism, the formal rate constant and potential of electrode reaction 3 are higher (in absolute values) in comparison to reaction 1.<sup>31</sup> Thus, a typical cyclic voltammogram features a single pair of peaks, encompassing reactions 1–3). Apart from voltammetry, reactions 1–3 were also investigated and confirmed with microscopic techniques.<sup>32,33</sup> In a complexing medium, an additional voltammetric response emerges due to reaction 4, where L is a complexing ligand.<sup>34</sup>



The formal potential of reaction 4 is usually more negative than reactions 1 and 3. It is important to note that a particular reaction mechanism is highly sensitive to the experimental conditions (pH, concentration, and composition of the aqueous electrolyte, type of working electrode, etc.) and can be significantly more complex than outlined above.<sup>35,36</sup>

## 2. EXPERIMENTAL SECTION

All chemicals used were of analytical grade purity (Sigma-Aldrich). Aqueous solutions were prepared with purified water obtained from an Arium mini-Plus purification system from Sartorius. PAA was in a noncross-linked form with a molar mass of 450,000 g/mol. The stock solution of PAA was prepared by dissolving 0.1 g in 10 mL of distilled water. Stock solutions of  $0.03 \text{ mol L}^{-1}$  copper(II) sulfate,  $0.5 \text{ mol L}^{-1}$  potassium nitrate, and  $0.1 \text{ mol L}^{-1}$  hydrogen peroxide were prepared in water. Accordingly, 1% (mass percent) of PAA solution at  $\text{pH} = 2.9$ , containing  $0.1 \text{ mol L}^{-1}$  potassium nitrate,

was the supporting electrolyte for the electrochemical study. Additionally, the concentration of copper(II) sulfate in the supporting electrolyte was  $3 \times 10^{-4} \text{ mol L}^{-1}$ . In the conventional experiments where  $\text{H}_2\text{O}_2$  was added to the supporting electrolyte, the concentration of  $\text{H}_2\text{O}_2$  varied from  $5 \times 10^{-3} \text{ mol L}^{-1}$  to  $1.5 \times 10^{-2} \text{ mol L}^{-1}$ . Experiments for studying the electrode mechanism were made with a glassy carbon as a working electrode, Ag/AgCl ( $3 \text{ mol L}^{-1} \text{ KCl}$ ) as a reference, and a carbon bar as a counter electrode. The electrolytic bridge connecting the reference electrode and the supporting electrolyte solution consisted of a  $0.5 \text{ mol L}^{-1} \text{ KNO}_3$  aqueous solution to avoid leaking of  $\text{Cl}^-$  and formation of copper complexes. The glassy carbon electrode was cleaned with  $\text{Al}_2\text{O}_3$  slurry, rinsed with water, and dried in the air prior to each experiment. All experiments were performed at room temperature, in air, and thus in the presence of dissolved oxygen, anticipating the analytical utility of the system for ambient gaseous  $\text{H}_2\text{O}_2$  detection in the future.

Experiments for gaseous  $\text{H}_2\text{O}_2$  detection were performed in a closed plastic chamber with a volume of 5 L using screen-printed carbon electrode (SPE) strips (Metrohm DropSens, 110) consisting of carbon as a working and counter electrode and Ag as a quasi-reference electrode. The aqueous solution of  $\text{H}_2\text{O}_2$  with a volume of 50 mL and concentrations from  $1 \times 10^{-4} \text{ mol L}^{-1}$  to  $1 \times 10^{-2} \text{ mol L}^{-1}$  was placed in the closed plastic chamber for a few hours before electrochemical measurements to establish equilibrium between the liquid and gas phases. Fifty microliters of the supporting electrolyte containing  $3 \times 10^{-4} \text{ mol L}^{-1}$  copper(II) sulfate were drop-casted on the SPE strip covering all three electrodes. Afterward, the modified SPE was inserted into the chamber and electrochemical measurements were performed after 1 min equilibration with the gaseous phase.

All electrochemical measurements were performed with an electrochemical measuring station  $\mu\text{Autolab}$  (potentiostat/galvanostat), model III, controlled by GPES software.

## 3. RESULTS AND DISCUSSION

**3.1. Studying the Basic Features of the Electrode Mechanism.** The supporting electrolyte consisting of 1% (mass percent) PAA and potassium nitrate has a pH close to 3, which indicates that only a fraction of carboxylic groups of

PAA is dissociated. Literature data indicate that  $\text{Cu}^{2+}$  ions are mainly in a hydrated form and less than 10% of dissolved  $\text{Cu}^{2+}$  ions are in a form of carboxylic complexes.<sup>37</sup> Thus, a typical voltammogram of  $\text{Cu}^{2+}$  ions in the studied supporting electrolyte at a glassy carbon electrode consists of a pair of voltammetric peaks, in accord with the electrode mechanism described with eqs 1–3 (Figure 1).

The broad, single cathodic peak reflects the electrode reductions of both  $\text{Cu}^{2+}$  and  $\text{Cu}^{1+}$  ions, affected by the chemical reaction 2, whereas the anodic peak represents the anodic stripping of the metallic copper deposited on the GC electrode surface. As the surface area of the anodic peak is smaller compared to the cathodic peak, it is possible that some of the reduced metallic copper are not deposited on the GC electrode surface, thus cannot be stripped from the electrode. Under corresponding experimental conditions, but in the absence of PAA, the cyclic voltammogram differs in the morphology of the anodic stripping peak. Specifically, it is significantly broader compared to PAA, while the anodic peak-current and peak-potential are virtually identical in both cases (data not shown). Thus, large polymeric molecules of PAA affect the morphology of the metal copper deposit, most likely causing the formation of a uniform metallic film. The morphology and peak current of the cathodic peak are also different (peak current is smaller with PAA); however, the cathodic peak potentials are comparable in both cases (data not shown).

As can be seen from Figure 1 (blue curve), the copper deposition gives rise to enhancement of the cathodic tail of the voltammogram at potentials more negative than  $-0.400$  V, implying an electrocatalytic effect toward the reduction of dissolved oxygen and/or hydrogen ions. It is important to note that an additional irreproducible reduction peak of a small intensity emerges at potentials around  $-0.325$  V, which might be associated with the reaction described with eq 4, where PAA is the complexing ligand. The latter reduction peak is most frequently covered with the baseline current.

Consecutive potential cycling shows that, after six cycles, a stable voltammogram is obtained, noting that the differences between the third and sixth cycles are minor (Figure 2).

Moreover, cleaning the GC electrode and repeating the voltammetric experiment result in a reproducible response, implying that the film growth stabilizes after several potential

cycles and can be completely removed from the electrode surface by mechanical cleaning. The relative simplicity and reproducibility of the voltammetric response under studied conditions indicate that no other copper oxides/hydroxides are formed, which is in accord with the theoretical Pourbaix diagrams of copper.<sup>38</sup>

Further insights into the mechanistic aspects of the reduction mechanism have been obtained by inspecting the role of the vertex potential ( $E_v$ ) at the side of negative potentials. The cyclic voltammetric response recorded from  $0.300$  V and a vertex potential more positive than  $-0.150$  V consist of a cathodic peak only (Figure 3).

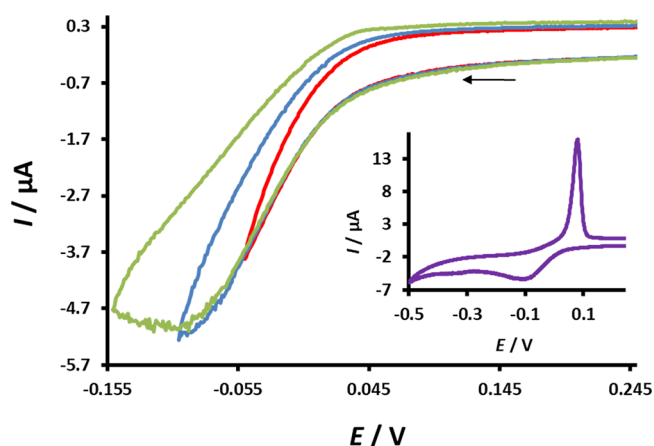


**Figure 3.** Typical cyclic staircase voltammograms for  $\text{Cu}^{2+}$  reduction recorded from the starting potential of  $0.300$  V by shifting the vertex potential ( $E_v$ ) from  $E_v = -0.050$  V (red),  $-0.100$  V (blue),  $-0.15$  V (green), and  $-0.500$  V (inset, violet curve). Other conditions are identical as in Figure 1.

For  $E_v = -0.150$  V (green curve in Figure 3), a very small anodic peak emerges, which progressively enlarges by shifting the vertex potential toward more negative values, eventually evolving to a strong anodic stripping peak for  $E_v = -0.500$  V (the inset of Figure 3, which represents the typical voltammetric response, shown also in Figures 1 and 2). Obviously, the elemental copper deposit on the GC electrode surface is not formed in a sufficient amount when the cyclic voltammetry is conducted at the scan rate of  $10$  mV/s with a vertex potential equal to or more positive than  $-0.150$  V. Under these conditions, the lack of any oxidation peak in cyclic voltammograms implies that  $\text{Cu}^+$  ions, as an intermediate species, are not stable and disproportionate according to reaction 2. Interestingly, in spite of the fact that one of the products of disproportionation reaction 2 is elemental copper, it cannot be electrochemically oxidized. This finding is in accordance with the previous finding that the surface area of the anodic peak is smaller compared to the cathodic peak (Figure 1). The most probable reason is that the elemental copper formed by homogeneous chemical reaction 2 is in a form of colloidal copper particles stabilized by PAA,<sup>39</sup> rather than being in a form of a metal deposit on the electrode surface. Thus, the copper deposit on the electrode surface is mainly formed by the electrode reaction 3. It should be noted that, besides reaction 2, the electrochemically formed  $\text{Cu}^+$  ions can be oxidized back to  $\text{Cu}^{2+}$  by dissolved oxygen (eq 5):

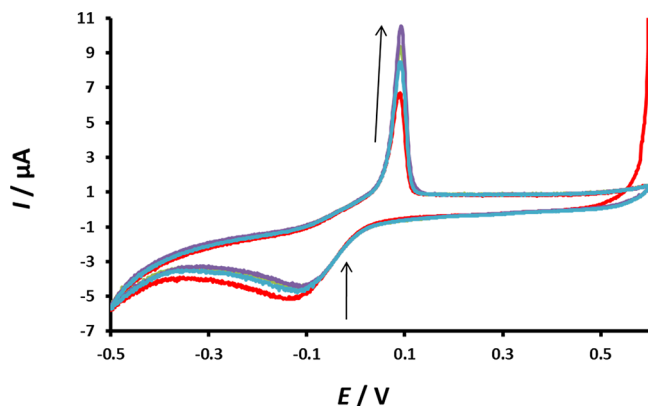
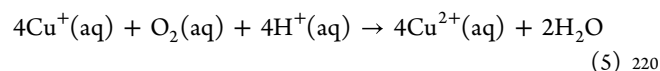


**Figure 2.** Consecutive cycles in cyclic staircase voltammetry, showing 1st, 2nd, 3rd, and 6th voltammograms. The direction of arrows indicates the change of the response by increasing the serial number of the potential cycle. Other conditions are identical as in Figure 1.

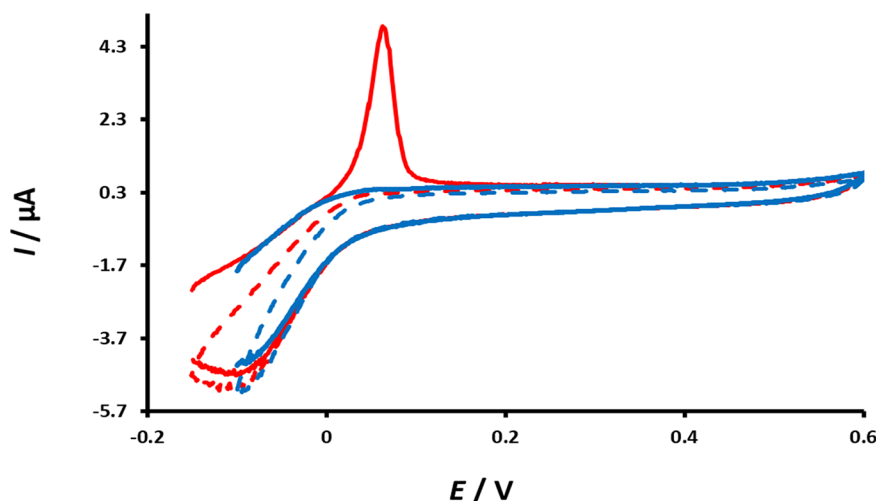


**Figure 4.** Cyclic staircase voltammograms recorded at the initial potential of  $-0.15$  V (red curve) and  $-0.1$  V (blue curve) with electrochemical deposition, at the initial potential, of 60 s. Dotted lines represent voltammograms without deposition. Other conditions are identical as in Figure 1.

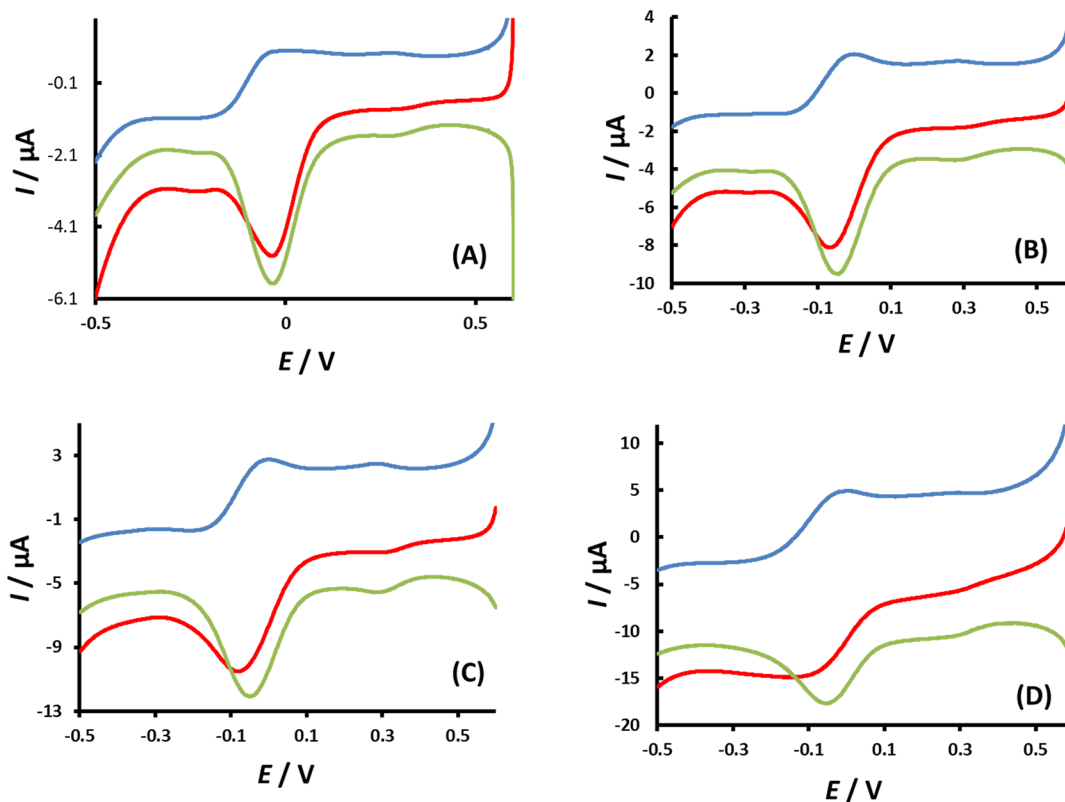


**Figure 5.** Typical square-wave voltammograms for the reduction of  $\text{Cu}^{2+}$  ions recorded with the frequency values of 1 Hz (A), 5 Hz (B), 10 Hz (C), and 50 Hz (D) showing forward (reduction, red curve), backward (oxidation, blue curve), and net (green curve) components at the starting potential  $E_{\text{start}} = 0.6$  V, SW amplitude  $E_{\text{sw}} = 50$  mV, and the step potential  $E_{\text{step}} = 1$  mV. Other conditions are identical as in Figure 1.

Yet, according to the literature data, reaction 5 is significantly slower than reaction 2.<sup>40</sup>

Further analysis of the critical potential and time required for producing copper deposit on the electrode surface according to electrode reaction 3 has been done by cyclic voltammetry starting at negative potentials. As illustrated in Figure 4, the intensity of the anodic stripping peak depends on both initial potential and deposition time.

For instance, a deposition process of 60 s at the potential of  $-0.150$  V results in a sufficient amount of copper deposit, thus enabling an anodic stripping peak to evolve (Figure 4, red

curve). Moreover, the blue voltammogram in Figure 4, recorded by deposition at  $-0.100$  V, is characterized with a small anodic stripping peak. Rigorously speaking, a small anodic stripping peak emerges even at deposition potentials more positive than  $-0.100$  V if the deposition time is sufficiently long. Thus, one can speculate that the formal potential of reaction 3 is more positive than reaction 1, which is in accord with the literature data.<sup>31</sup>

The complexity of this two-step electron transfer mechanism arises additionally from the fact that the intermediary species  $\text{Cu}^+$  are competitively consumed by the homogeneous redox

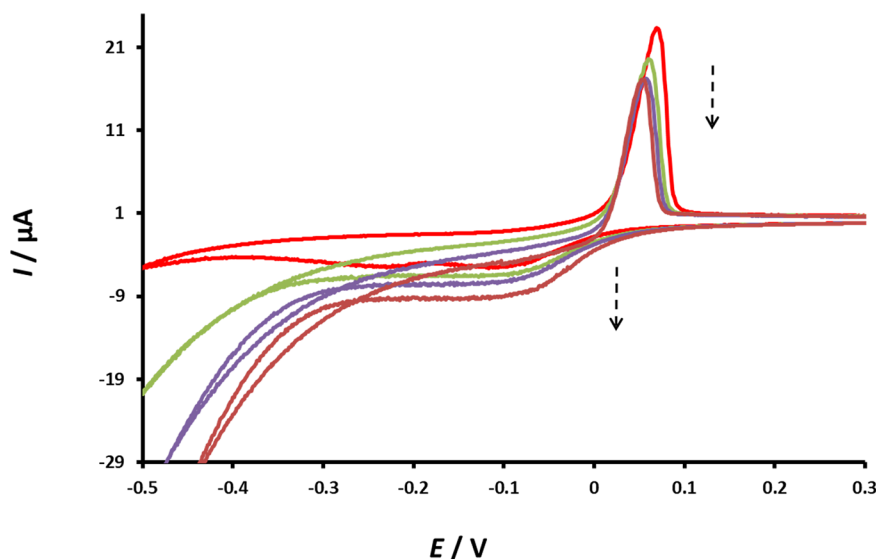


**Figure 6.** Effect of the increasing concentration of  $\text{H}_2\text{O}_2$  on the cyclic staircase voltammetric response of  $\text{Cu}^{2+}$  ions. The red voltammogram shows the response of  $\text{Cu}^{2+}$  without  $\text{H}_2\text{O}_2$ . The arrows indicate the variation of the response by adding  $\text{H}_2\text{O}_2$  at concentrations of  $5 \times 10^{-3}$ ,  $1 \times 10^{-2}$ , and  $1.5 \times 10^{-2} \text{ mol L}^{-1}$ . Other conditions are identical as in Figure 1.

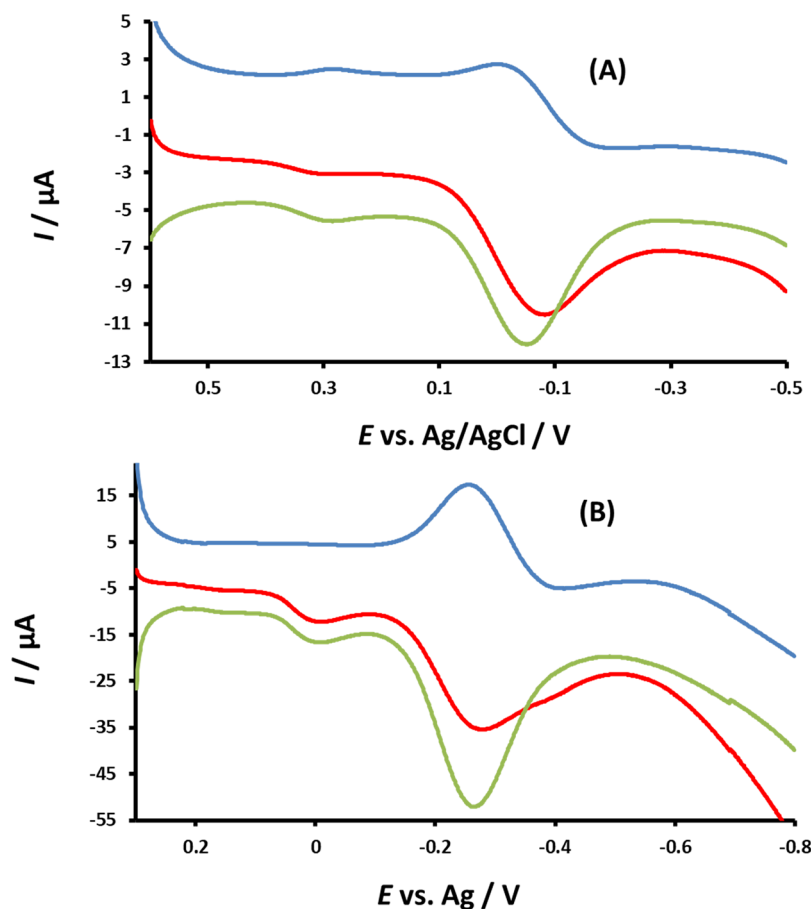


**Figure 7.** Typical SW voltammograms for the reduction of  $\text{Cu}^{2+}$  at glassy carbon (A) and the screen-printed carbon electrode (B), showing forward (red), backward (blue), and net (green) voltammograms. SW frequency is 10 Hz, and other potential modulation parameters are identical as in Figure 5. The silver wire serves as a pseudo reference electrode in (B). Other conditions are identical as in Figure 1.

reactions 2 and the electrode reaction 3 (while the rate of reaction 5 is assumed to be insignificant compared to reaction 2<sup>40</sup>). Cyclic voltammetry conducted at scan rates up to 200 mV/s, within the potential window from 0.300 V to −0.150 V

(data not shown), does not result in an anodic peak due to electrochemical reoxidation of  $\text{Cu}^+$  to  $\text{Cu}^{2+}$ , which indicates that the rate of reaction 2 is relatively high. Using however SWV, as a significantly faster technique, an anodic peak

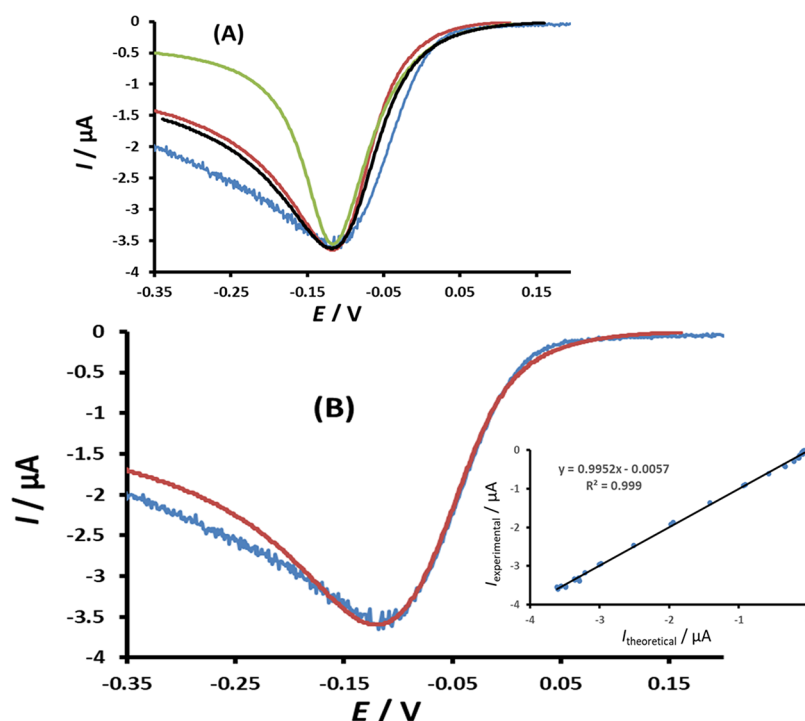


**Figure 8.** (A) Comparison of the experimental (blue line) with theoretical voltammograms considering the cathodic peak of the cyclic staircase voltammetry. Simulation conditions are:  $T = 298.15$  K, electron transfer coefficient  $\alpha = 0.5$ , and step potential  $dE = 1$  mV. The other conditions specific for each theoretical voltammogram are:  $\kappa = 1$ ,  $\Delta E = -0.2$  V, and  $k_c = 10^5$  s $^{-1}$  (red line);  $\kappa = 0.398$ ,  $\Delta E = 0$  V, and  $k_c = 10^5$  s $^{-1}$  (green line); and  $\kappa = 0.398$ ,  $\Delta E = -0.2$  V, and  $k_c = 10^7$  s $^{-1}$  (black line). (B) The best fit between experimental (blue line) and theoretical (red line) found for  $\kappa = 0.398$ ,  $\Delta E = -0.2$  V, and  $k_c < 10^5$  s $^{-1}$ . The inset shows the linearity of the best fit in potential interval from 0.15 V to  $-0.168$  V. Experimental conditions are identical as in Figure 1.

emerges by increasing the frequency of potential modulation (Figure 5).

The backward, anodic component of the SW voltammetric response has a diffusion-affected character, rather than being an anodic stripping peak. Its intensity enlarges relative to the forward (reductive) component in proportion to the frequency. Hence, it corresponds to the electrochemical oxidation of  $\text{Cu}^+$  back to  $\text{Cu}^{2+}$  ions, circumventing the effect of the chemical reaction 2. To get an impression of the critical time window of the SW voltammetric experiment, let us note that the duration of a single SW potential pulse, for instance at 50 Hz, is only 10 ms.<sup>41</sup> In the course of two adjacent pulses (i.e., within the time interval of 20 ms), the reduction of  $\text{Cu}^{2+}$  and reoxidation of electrochemically formed  $\text{Cu}^+$  ions take place, thus rendering homogenous chemical reaction 2 less effective. The appearance of an anodic peak in the SW voltammograms at higher frequencies also implies that  $\text{Cu}^+$  ions are not instantly transformed electrochemically to  $\text{Cu(s)}$  according to reaction 3, indicating a degree of stabilization within the polymer molecules of PAA.

Addition of  $\text{H}_2\text{O}_2$  to the experimental system increases the reduction peak in CSV, most probably as a consequence of an EC' reaction pathway (Figure 6).<sup>42–44</sup>

In the presence of  $\text{H}_2\text{O}_2$ , the reduction current starts increasing even at positive potentials of 0.050 V (cf. Figure 6), transforming the cathodic peak into a sigmoid curve. Hence, it is plausible to assume that the redox couple  $\text{Cu}^{2+}/\text{Cu}^+$  acts as a redox mediator for the indirect electrochemical reduction of  $\text{H}_2\text{O}_2$ . Moreover, at potentials more negative than  $-0.300$  V, a strong increase of the reduction current tail occurs, associated with direct  $\text{H}_2\text{O}_2$  reduction on the copper-modified GC

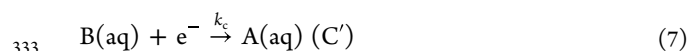
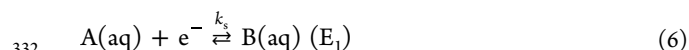
electrode. Interestingly, the reduction tail does not form a voltammetric peak at more negative potentials (data not shown) indicating that the electrode process is not limited by the diffusional mass transfer of hydrogen peroxide. Most likely a complex radical-type electrode mechanism takes place initiated by the reduction of  $\text{H}_2\text{O}_2$  on the metallic copper particles, involving further the aqueous phase in the overall electrode mechanism.<sup>44,45</sup>

Mechanistic considerations at GCE are expected to be similar at screen-printed carbon electrodes, anticipating a plausible difference in the kinetics of both electrode reactions 1 and 3. Figure 7 compares typical SW voltammograms for the reduction of  $\text{Cu}^{2+}$  ions at two electrodes.

Evidently, the absolute current and potential values are not directly comparable owing to the discrepancies between the working electrode surface area and reference electrodes (i.e., Ag/AgCl (3 mol L $^{-1}$  KCl) and a silver wire for GCE and SPE, respectively). Yet, a comparison of the relative parameters, such as the ratio of the peak currents of the forward and backward SW voltammetric components ( $I_{p,f}/I_{p,b}$ ), is highly indicative of mechanistic considerations. Specifically, the ratio is  $I_{p,f}/I_{p,b} = 10$  and 1.5 for GCE and SPE, respectively. The anodic, backward voltammetric component assigned to the electrochemical reoxidation  $\text{Cu}^+$  to  $\text{Cu}^{2+}$  is significantly more developed at SPE (cf. Figure 7). Apparently, the stability of  $\text{Cu}^+$  in the vicinity of the electrode is more pronounced at SPE than at GCE. Considering that the composition of the medium is identical for both electrodes, the only reason for such obvious differences arises from the slower electrode kinetics of the second electrode reaction 3, which competitively exhausts  $\text{Cu}^+$  ions in parallel with the reaction 2. The last conclusion is

in favor of the analytical detection of  $\text{H}_2\text{O}_2$  on an SPE via an EC' mechanism where the  $\text{Cu}^{2+}/\text{Cu}^+$  couple serves as a redox mediator.

**3.2. Theoretical Consideration and Simulations of the Electrode Mechanism.** To provide further insights into the complex voltammetric features of the studied electrode mechanism, the voltammetric outcome was briefly analyzed using numerical simulations. In a first approximation, an  $\text{E}_1\text{C}'\text{E}_2$  reaction mechanism has been assumed at a planar electrode of dissolved species, considering semi-infinite diffusional mass transport (eqs 6–8). The first electron transfer step  $\text{E}_1$  (eq 6), corresponding to the reduction of  $\text{Cu}^{2+}$  to  $\text{Cu}^+$  (eq 1), is assumed to be electrochemically quasireversible, whereas the second electrode reaction  $\text{E}_2$  (eq 8), which corresponds to the reduction of  $\text{Cu}^+$  to  $\text{Cu}(0)$  (eq 3), is simulated as being electrochemically reversible. To tackle the mathematical complexity of the experimental system, the disproportionation reaction of  $\text{Cu}^+$  ions (eq 3) is assimilated as being a simple, regenerative reaction  $\text{C}'$  (eq 7).<sup>46</sup>



Details on the mathematical modeling by means of the step-function method are given elsewhere.<sup>41</sup>

Initial simulations have been focused on understanding the morphology and evolution of the cathodic peak under conditions of cyclic staircase voltammetry (cf. Figures 1–4). Critical parameters controlling the voltammetric response are the electrode kinetic parameter of the first electrode reaction  $\kappa$ , the potential difference between the formal reduction potentials of the first and the second electrode reaction,  $\Delta E = E^{\ominus}_1 - E^{\ominus}_2$ , and the rate constant  $k_c$  ( $\text{s}^{-1}$ ) of the regenerative chemical reaction  $\text{C}'$  (eq 7). The electrode kinetic parameter controlling the electrochemical reversibility of the first electrode reaction is defined as  $\kappa = k_s \sqrt{\frac{\tau}{D}}$ , where  $k_s$  is the standard rate constant ( $\text{cm s}^{-1}$ ),  $\tau$  is the duration of a single potential tread in staircase voltammetry, and  $D$  is the common diffusion coefficient. All three parameters  $\kappa$ ,  $\Delta E$ , and  $k_c$  have been systematically studied, over a broad range of values. Specifically, the first electrode reaction was assumed to be typically quasireversible characterized by the electrode kinetic parameter within the interval  $-0.42 \leq \log(\kappa) \leq 0.40$ ; the potential difference was varied from  $\Delta E = 0.200$  V (meaning that the formal reduction potential of the second electrode reaction is more negative than the first one) to  $\Delta E = -0.300$  V typical for an  $\text{E}_1\text{E}_2$  mechanism with inverted potentials,<sup>47</sup> as expected for the copper system, and the catalytic rate constant was altered over the interval  $\log(k_c/\text{s}^{-1}) \leq 11$ .

Under conditions of cyclic staircase voltammetry, when the simulation was conducted at a relatively slow scan rate of  $\nu = 10$  mV/s (corresponding to the conditions of Figure 1), the morphology of the cathodic peak depends predominantly on the value of  $\Delta E$  and  $\kappa$ , as shown in Figure 8A.

The best fit is achieved by assuming a mechanism with inverted formal reduction potentials, i.e.,  $\Delta E = -0.200$  V and the electrode kinetic parameter of  $\kappa = 0.398$  (Figure 8B). Under these conditions, the intensity of the response is virtually identical regardless of the kinetics of the chemical reaction over the interval  $k_c < 10^5 \text{ s}^{-1}$ , implying that the rate of

the chemical reaction cannot be unambiguously estimated and the voltammetric features are predominantly controlled by the inverted potential difference of  $\Delta E = -0.200$  V. Let us note that, in a pure aqueous medium, the potential difference between reactions 1 and 3 is  $\Delta E = -0.361$  V. Thus,  $\text{Cu}^+$  ions are significantly stabilized in the presence of PAA.

Fitting the dimensionless theoretical current function defined as  $\psi = I/A$ , with the experimental current ( $I$ ), the value of the amperometric constant  $A = 2.35 \times 10^{-5}$  A was found by the simulations. Let us note that the amperometric constant is defined as  $A = nFSc^*(D/\tau)^{1/2}$ , where  $n$  is the number of electrons in a single electron transfer step,  $F$  is the Faraday constant,  $S$  is the electrode surface area, and  $c^*$  is the bulk concentration of the initial reactant. Knowing that  $n = 1$ ,  $S = 7.1 \times 10^{-2} \text{ cm}^2$ ,  $c^* = 3 \times 10^{-4} \text{ mol dm}^{-3}$ , and  $\tau = 0.1$  s, the diffusion coefficient estimated from the value of the amperometric constant is  $D = 1.3 \times 10^{-5} \text{ cm}^2/\text{s}$ , which is in excellent agreement with the literature data.<sup>30</sup> Thus, from the definition of the electrode kinetic parameter  $\kappa = k_s \sqrt{\frac{\tau}{D}}$  and value of  $\kappa = 0.398$  found by fitting procedure, the estimated value of the standard rate constant is  $k_s = 4.5 \times 10^{-3} \text{ cm s}^{-1}$ . The inset of Figure 8B shows the simple correlation between theoretical and experimental data in the potential interval from 0.150 V to  $-0.168$  V, represented by a linear regression line ( $R^2 = 0.999$ ) with a slope close to 1 and an intercept close to zero, inferring high reliability of the estimated parameters.

Further simulations have been conducted by SWV, attempting to get an impression of the value of the chemical rate constant  $k_c$  (rigorously speaking, it is an apparent rate constant, as the real disproportionation reaction (eq 2) is approximated as a first-order regenerative chemical reaction (eq 7). The value of  $k_c$  has been systematically altered over the interval  $0 \leq \log(k_c/\text{s}^{-1}) \leq 5$ , for three SW frequencies of 5, 10, and 50 Hz. The other parameters have been set to the values estimated in previous simulations (i.e.,  $k_s = 4.5 \times 10^{-3} \text{ cm s}^{-1}$ ,  $D = 1.3 \times 10^{-5} \text{ cm}^2/\text{s}$ , and  $\Delta E = -0.200$  V). Comparing the morphological evolution of the forward and backward SW voltammetric components with the frequency, it has been established that the experimental voltammograms presented in Figure 5 can be reproduced assuming a value of the chemical rate constant to fall within the interval  $2 \leq \log(k_c/\text{s}^{-1}) \leq 3$ . To the best of our knowledge, kinetic information on the disproportionation reaction in an aqueous medium was not reported so far. The main reason is that the reaction is extremely fast, and only the equilibrium constant in the order of  $10^6$  was estimated.<sup>48</sup> In the present system, although the rate constant is roughly estimated, the value suggests certain stabilization of  $\text{Cu}^+$  by PAA.

**3.3. Analytical Application.** Physicochemical properties of PAA, i.e., its ability to absorb gases, and small volume of the hydrogel on screen-printed electrodes should enable a high concentration of  $\text{H}_2\text{O}_2$  and at the same time offer high chemical stability in the gel phase and fast equilibration of  $\text{H}_2\text{O}_2$  on the gas/liquid interface. For this reason, SPE was modified with a 50  $\mu\text{L}$  aqueous solution of PAA, containing  $\text{KNO}_3$  and  $\text{Cu}^{2+}$  ions. The modified SPE was inserted in the chamber containing gaseous  $\text{H}_2\text{O}_2$ , with a previously established equilibrium between the liquid and gas phases. Electrochemical measurements were performed after 1 min equilibration with the gaseous phase.

Concentration analysis has been done over the interval from 0.1 mmol/L to 10 mmol/L, taking into account the

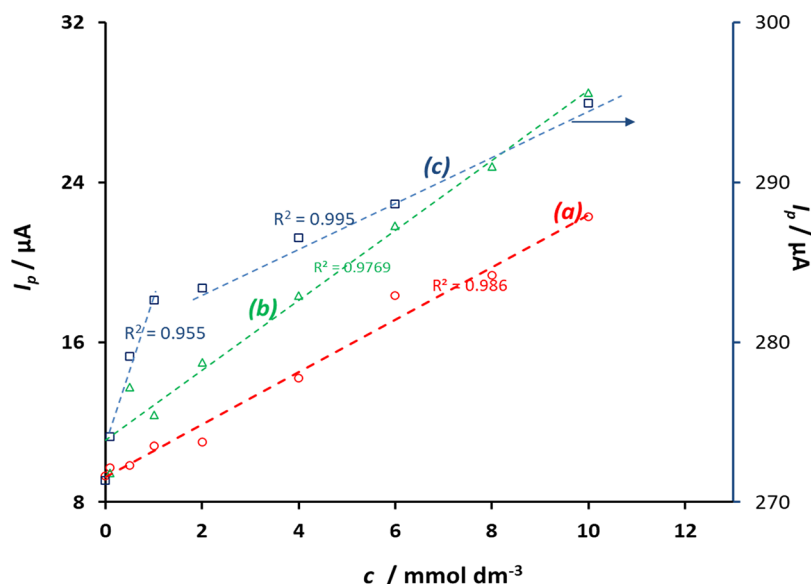


**Figure 9.** Calibration curves constructed for different concentrations of aqueous solutions of  $\text{H}_2\text{O}_2$  in the chamber using SPE at  $T = 303$  K. Electrochemical signal was measured after a 1 min equilibration period of the modified SPE in the chamber using cyclic staircase voltammetry (a), chronoamperometry (b), and SW voltammetry (c, right ordinate). For CSV:  $\nu = 50$  mV/s,  $E_{\text{step}} = 5$  mV,  $E_1 = 0.3$  V, (third potential scan used for calibration line). For SWV:  $E_{\text{sw}} = 50$  mV,  $f = 10$  Hz,  $E_{\text{step}} = 1$  mV,  $E_1 = 0.3$  V. For CA:  $E = -0.4$  V,  $t = 10$  s. For all techniques: SPCE—working electrode, Ag—reference electrode. Other conditions are identical as in Figure 1.

**Table 1. Limit of Detection (LOD) and Limit of Quantification (LOQ) for Gaseous  $\text{H}_2\text{O}_2$  Measured with CSV, SWV, and CA on an SPE<sup>a</sup>**

technique	LOD (gaseous $\text{H}_2\text{O}_2$ ) $/\mu\text{g dm}^{-3}$	LOQ (gaseous $\text{H}_2\text{O}_2$ ) $/\mu\text{g dm}^{-3}$
CV	$3.49 \cdot 10^{-2}$	$1.16 \cdot 10^{-1}$
CA	$4.58 \cdot 10^{-2}$	$1.51 \cdot 10^{-1}$
SWV	$1.44 \cdot 10^{-1}$	$4.75 \cdot 10^{-1}$

<sup>a</sup>Other conditions are identical as in Figure 9.

effect of both redox reactions of  $\text{H}_2\text{O}_2$  and disproportionation of  $\text{Cu}^+$ .

#### 4. CONCLUSIONS

To the best of our knowledge, it is the first mechanistic analysis of copper(II) reduction in PAA aqueous solution using voltammetric techniques. Experimental data, together with the theoretical considerations and simulations of the voltammetric response, confirm that the reaction pathway is similar to in a pure aqueous medium, with indications that the intermediate  $\text{Cu}^+$  ions are partly stabilized by PAA, and their further reduction is thermodynamically less favored, while the kinetics of their disproportionation is diminished in comparison to a pure aqueous medium. Moreover, at commercially available carbon SPE, the reduction of  $\text{Cu}^+$  to the elemental copper is electrochemically slower than at GCE, which is beneficial for analytical purposes for  $\text{H}_2\text{O}_2$  detection where the  $\text{Cu}^{2+}/\text{Cu}^+$  couple serves as a redox mediator. SPE covered with a thin film of 50  $\mu\text{L}$  aqueous solution of PAA, containing  $\text{KNO}_3$  and  $\text{Cu}^{2+}$  ions, is evidently a promising platform for detection of gaseous  $\text{H}_2\text{O}_2$  in the presence of oxygen with a superior limit of detection ranging in the sub- $\mu\text{g dm}^{-3}$  concentration level.

concentration of the aqueous solution of  $\text{H}_2\text{O}_2$  inserted in the gas chamber. The corresponding concentration interval for the gaseous  $\text{H}_2\text{O}_2$  is  $7.27 \cdot 10^{-8}$ – $7.27 \cdot 10^{-6}$  mmol/L, estimated utilizing Henry's law.<sup>49,50</sup> Calibration curves were constructed and compared for cyclic staircase voltammetry, chronoamperometry, and square-wave voltammetry (Figure 9).

For the calibration line constructed by CSV, the reduction peak-current was measured by applying a tangent to estimate the background current (Figure 9, curve a). In SWV, the absolute peak current values of the net component were measured. The concentration dependence under conditions of SWV (Figure 9, curve c) is more complex. The dependence can be linearized over two separate concentration intervals, i.e., from 0 mmol/L to 1 mmol/L ( $R^2 = 0.9545$ ) and from 1 mmol/L to 10 mmol/L ( $R^2 = 0.9946$ ). The complexity of the concentration analysis with SWV clearly reflects the underlying complexity of the electrode mechanism, most likely due to the competition of the redox reactions of  $\text{H}_2\text{O}_2$  with  $\text{Cu}^+$  ions and the disproportionation reaction 2.

The calibration line constructed by CA is based on current values measured at a potential of  $-0.400$  V (vs Ag-pseudo-reference electrode, cf. Figure 7B) after 10 s. The limit of detection (LOD) and the limit of quantification (LOQ) were calculated for gaseous  $\text{H}_2\text{O}_2$  according to  $\text{LOD} = 3 \cdot S_a/b$  and  $\text{LOQ} = 10 \cdot S_a/b$ , where  $S_a$  is the standard deviation of the response of the linear regression and  $b$  is the slope of the calibration line (Table 1).

Although the overall reaction pathway of  $\text{Cu}^{2+}$  reduction in the presence of hydrogen peroxide does not depend on the electrochemical technique applied, the differences in potential modulation and the critical time of the electrochemical experiment cause different aspects of the complex mechanism to prevail under given conditions; thus, differences in the analytical outcome are likely. For instance, the critical time window is in the millisecond range for the experiment under conditions of SWV, while it is in a second range for CSV and CA experiments, which is critically important for the overall

## AUTHOR INFORMATION

## Corresponding Author

Valentin Mirceski – Institute of Chemistry, Faculty of Natural Sciences and Mathematics, “Ss Cyril and Methodius” University in Skopje, Skopje 1000, North Macedonia; Department of Inorganic and Analytical Chemistry, University of Lodz, Lodz 91-403, Poland; Research Center for Environment and Materials, Macedonian Academy of Sciences and Arts, Skopje 1000, North Macedonia; [orcid.org/0000-0002-9191-3926](https://orcid.org/0000-0002-9191-3926); Email: [valentin@pmf.ukim.mk](mailto:valentin@pmf.ukim.mk)

## Authors

Leon Stojanov – Institute of Chemistry, Faculty of Natural Sciences and Mathematics, “Ss Cyril and Methodius” University in Skopje, Skopje 1000, North Macedonia; [orcid.org/0000-0001-7528-654X](https://orcid.org/0000-0001-7528-654X)

Angela Rafailovska – Institute of Chemistry, Faculty of Natural Sciences and Mathematics, “Ss Cyril and Methodius” University in Skopje, Skopje 1000, North Macedonia

Vasko Jovanovski – Department of Materials Chemistry, National Institute of Chemistry, Ljubljana 1000, Slovenia

Complete contact information is available at:

<https://pubs.acs.org/10.1021/acs.jpcc.2c05259>

## Notes

The authors declare no competing financial interest.

## ACKNOWLEDGMENTS

The authors would like to acknowledge with gratitude the support from the National Science Centre of Poland through the Opus Lap grant no. 2020/39/I/ST4/01854.

## REFERENCES

- (1) Abdelaal, M. Y.; Makki, M. S. I.; Sobahi, T. R. A. Modification and characterization of polyacrylic acid for metal ion recovery. *Am. J. Polym. Sci.* **2012**, *2*, 73–78.
- (2) Nho, Y.-C.; Park, J.-S.; Lim, Y.-M. Preparation of poly(acrylic acid) hydrogel by radiation crosslinking and its application for mucoadhesives. *Polymer* **2014**, *6*, 890–898.
- (3) Yin, M. J.; Yao, M.; Gao, S.; Zhang, A. P.; Tam, H. Y.; Wai, P. K. A rapid 3D patterning of poly (acrylic acid) ionic hydrogel for miniature pH sensors. *Adv. Mater.* **2016**, *28*, 1394–1399.
- (4) Bastakoti, B. P.; Guragain, S.; Nakashima, K.; Yamauchi, Y. Stimuli-induced core–corona inversion of micelle of poly(acrylic acid)-block-poly(N-isopropylacrylamide) and its application in drug delivery. *Macromol. Chem. Phys.* **2015**, *216*, 287–291.
- (5) Braam, K.; Subramanian, V. Astencil printed, high energy density silver oxide battery using a novel photopolymerizable poly(acrylic acid) separator. *Adv. Mater.* **2015**, *27*, 689–694.
- (6) Zhao, Q.; Yin, M.; Zhang, A. P.; Prescher, S.; Antonietti, M.; Yuan, J. Hierarchically structured nanoporous poly (ionic liquid) membranes: Facile preparation and application in fiber-optic pH sensing. *J. Am. Chem. Soc.* **2013**, *135*, 5549–5552.
- (7) Zhao, Q.; Dunlop, J. W. C.; Qiu, X.; Huang, F.; Zhang, Z.; Heyda, J.; Dzubiella, J.; Antonietti, M.; Yuan, J. An instant multi-responsive porous polymer actuator driven by solvent molecule sorption. *Nat. Commun.* **2014**, *5*, 1–8.
- (8) Zhao, C.; Nie, S.; Tang, M.; Sun, S. Polymeric pH-sensitive membranes—A review. *Prog. Polym. Sci.* **2011**, *36*, 1499–1520.
- (9) Yin, M. J.; Wu, C.; Shao, L. Y.; Chan, W. K. E.; Zhang, A. P.; Lu, C.; Tam, H. Y. Label-free, disposable fiber-optic biosensors for DNA hybridization detection. *Analyst* **2013**, *138*, 1988–1994.
- (10) Gu, B.; Yin, M. J.; Zhang, A. P.; Qian, J. W.; He, S. Fiber-optic metal ion sensor based on thin-core fiber modal interferometer with nanocoating self-assembled via hydrogen bonding. *Sens. Actuators, B* **2011**, *160*, 1174–1179.
- (11) Pearson, A. C.; Linford, M. R.; Harb, J. N.; Davis, R. C. Dual patterning of a poly (acrylic acid) layer by electron-beam and block copolymer lithographies. *Langmuir* **2013**, *29*, 7433–7438.
- (12) Chiang, E. N.; Dong, R.; Ober, C. K.; Baird, B. A. Cellular responses to patterned poly (acrylic acid) brushes. *Langmuir* **2011**, *27*, 7016–7023.
- (13) Hwang, I. T.; Oh, M. S.; Jung, C. H.; Choi, J. H. Direct patterning of poly (acrylic acid) on polymer surfaces by ion beam lithography for the controlled adhesion of mammalian cells. *Biotechnol. Lett.* **2014**, *36*, 2135–2142.
- (14) Wang, Y. M.; Cui, Y.; Cheng, Z. Q.; Song, L. S.; Wang, Z. Y.; Han, B. H.; Zhu, J. S. Poly (acrylic acid) brushes pattern as a 3D functional biosensor surface for microchips. *Appl. Surf. Sci.* **2013**, *266*, 313–318.
- (15) Mandel, M. The potentiometric titration of weak polyacids. *Eur. Polym. J.* **1970**, *6*, 807–822.
- (16) Terao, K. Poly(acrylic acid) (PAA). Kobayashi, S.; Müllen, K., Eds.; *Encyclopedia of Polymeric Nanomaterials*; Springer: Berlin, Heidelberg, 2014; DOI: [10.1007/978-3-642-36199-9\\_279-1](https://doi.org/10.1007/978-3-642-36199-9_279-1).
- (17) Swift, T.; Swanson, L.; Geoghegan, M.; Rimmer, S. The pH-responsive behaviour of poly (acrylic acid) in aqueous solution is dependent on molar mass. *Soft Matter* **2016**, *12*, 2542–2549.
- (18) Isailović, J.; Vidović, K.; Hočevar, S. B. Simple electrochemical sensors for highly sensitive detection of gaseous hydrogen peroxide using polyacrylic-acid-based sensing membrane. *Sens. Actuators, B* **2022**, *352*, No. 131053.
- (19) Wang, Z.; Wang, Z.; Zhang, H.; Duan, X.; Xu, J.; Wen, Y. Electrochemical sensing application of poly (acrylic acid modified EDOT-co-EDOT): PSS and its inorganic nanocomposite with high soaking stability, adhesion ability and flexibility. *RSC Adv.* **2015**, *5*, 12237–12247.
- (20) Ricardo Teixeira Tarley, C.; de Cássia Mendonça, J.; Rianne da Rocha, L.; Boareto Capelari, T.; Carolyne Prete, M.; Cecílio Fonseca, M.; Midori de Oliveira, M.; César Pereira, A.; Luiz Scheel, G.; Bastos Borges, K.; Gava Segatelli, M. Development of a molecularly imprinted poly (acrylic acid)-mwcnt nanocomposite electrochemical sensor for tramadol determination in pharmaceutical samples. *Electroanalysis* **2020**, *32*, 1130–1137.
- (21) Loukides, S.; Horvath, I.; Wodehouse, T.; Cole, P. J.; Barnes, P. J. Elevated levels of expired breath hydrogen peroxide in bronchiectasis. *Am. J. Respir. Crit. Care Med.* **1998**, *158*, 991–994.
- (22) Sznajder, J. I.; Fraiman, A.; Hall, J. B.; Sanders, W.; Schmidt, G.; Crawford, G.; Nahum, A.; Factor, P.; Wood, L. D. H. Increased hydrogen peroxide in the expired breath of patients with acute hypoxemic respiratory failure. *Chest* **1989**, *96*, 606–612.
- (23) Mucci, N.; Dugheri, S.; Bonari, A.; Farioli, A.; Rapisarda, V.; Garzaro, G.; Cappelli, G.; Arcangeli, G. Health risk assessment related to hydrogen peroxide presence in the workplace atmosphere: analytical methods evaluation for an innovative monitoring protocol. *Int. J. Occup. Med. Environ. Health* **2020**, *33*, 137–150.
- (24) Chen, Q.; Yang, L.; Guo, K.; Yang, J.; Han, J. M. Expedite Fluorescent Sensor Prototype for Hydrogen Peroxide Detection with Long-Life Test Substrates. *ACS Omega* **2021**, *6*, 11447–11457.
- (25) Zhu, H.; Zhang, S.; Li, M.; Shao, Y.; Zhu, Z. Electrochemical sensor for melamine based on its copper complex. *Chem. Commun.* **2010**, *46*, 2259–2261.
- (26) Ye, W.; Guo, X.; Ma, T. A review on electrochemical synthesized copper-based catalysts for electrochemical reduction of CO<sub>2</sub> to C<sub>2</sub><sup>+</sup> products. *Chem. Eng. J.* **2021**, *414*, No. 128825.
- (27) Welch, C. M.; Compton, R. G. The use of nanoparticles in electroanalysis: a review. *Anal. Bioanal. Chem.* **2006**, *384*, 601–619.
- (28) Evans, J.; Pletcher, D.; Warburton, P. R. G.; Gibbs, T. K. A new electrochemical sensor for carbon dioxide: Part 2. Study of the sensor chemistry. *J. Electroanal. Chem. Interfacial Electrochem.* **1989**, *262*, 119–129.

- (29) Altermatt, J. A.; Manahan, S. E. Electrochemical behavior of cuprous ion in a noncomplexing aqueous medium. *Anal. Chem.* **1968**, *40*, 655–657.
- (30) Tindall, G. W.; Bruckenstein, S. Determination of heterogeneous equilibrium constants by chemical stripping at a ring-disk electrode. Evaluation of the equilibrium constant for the reaction copper + copper(II) → 2copper(I) in 0.2M sulfuric acid. *Anal. Chem.* **1968**, *40*, 1402–1404.
- (31) Mattsson, E.; Bockris, J. O'. M. Galvanostatic studies of the kinetics of deposition and dissolution in the copper + copper sulphate system. *Trans. Faraday Soc.* **1959**, *55*, 1586–1601.
- (32) Grujicic, D.; Pesic, B. Reaction and nucleation mechanisms of copper electrodeposition from ammoniacal solutions on vitreous carbon. *Electrochim. Acta* **2005**, *50*, 4426–4443.
- (33) Grujicic, D.; Pesic, B. Electrodeposition of copper: the nucleation mechanisms. *Electrochim. Acta* **2002**, *47*, 2901–2912.
- (34) Bolzán, A. E. Electrodeposition of copper on glassy carbon electrodes in the presence of picolinic acid. *Electrochim. Acta* **2013**, *113*, 706–718.
- (35) Cheng, B.; Yi, H.; He, C.; Liu, C.; Lei, A. Revealing the ligand effect on copper(I) disproportionation via operando IR spectra. *Organometallics* **2015**, *34*, 206–211.
- (36) Rosen, B. M.; Jiang, X.; Wilson, C. J.; Nguyen, N. H.; Monteiro, M. J.; Percec, V. The disproportionation of Cu(I)X mediated by ligand and solvent into Cu(0) and Cu(II)X<sub>2</sub> and its implications for SET-LRP. *J. Polym. Sci., Part A: Polym. Chem.* **2009**, *47*, 5606–5628.
- (37) Chevtsev, A. S.; Tabunshchikov, A. I.; Ozerin, A. S.; Radchenko, F. S.; Novakov, I. A. Interaction of Polyacrylic Acid with Copper, Cobalt, and Nickel Ions in Aqueous Solutions. *Russ. J. Gen. Chem.* **2020**, *90*, 870–873.
- (38) Takeno, N. Atlas of Eh-pH diagrams. *Geol. Surv. Jpn. Open File Rep.* **2005**, *419*, 102.
- (39) Guo, H.; Chen, Y.; Cortie, M. B.; Liu, X.; Xie, Q.; Wang, X.; Peng, D. L. Shape-selective formation of monodisperse copper nanospheres and nanocubes via disproportionation reaction route and their optical properties. *J. Phys. Chem. C* **2014**, *118*, 9801–9808.
- (40) Papassiopi, N.; Gaunand, A.; Renon, H. Oxidation of Cu(I) by oxygen in concentrated NaCl solutions—I. Homogeneous kinetics of oxidation by molecular oxygen in solution. *Chem. Eng. Sci.* **1985**, *40*, 1527–1531.
- (41) Mirčeski, V.; Komorsky-Lovrić, S.; Lovrić, M. *Square-wave voltammetry: Theory and application*; Springer: Berlin, 2007; DOI: 10.1007/978-3-540-73740-7.
- (42) Skinner, J. F.; Glasel, A.; Hsu, L. C.; Funt, B. L. Rotating ring disk electrode study of the hydrogen peroxide oxidation of Fe(II) and Cu(I) in hydrochloric acid. *J. Electrochem. Soc.* **1980**, *127*, 315.
- (43) Nicol, M. J. Kinetics of the oxidation of copper(I) by oxygen in acidic chloride solutions. *S. Afr. J. Chem.* **1984**, *37*, 77–80.
- (44) Masarwa, M.; Cohen, H.; Meyerstein, D.; Hickman, D. L.; Bakac, A.; Espenson, J. H. Reactions of low-valent transition-metal complexes with hydrogen peroxide. Are they "Fenton-like" or not? 1. The case of Cu<sup>+</sup> aq and Cr<sup>2+</sup> aq. *J. Am. Chem. Soc.* **1988**, *110*, 4293–4297.
- (45) Pham, A. N.; Xing, G.; Miller, C. J.; Waite, T. D. Fenton-like copper redox chemistry revisited: Hydrogen peroxide and superoxide mediation of copper-catalyzed oxidant production. *J. Catal.* **2013**, *301*, 54–64.
- (46) Song, P.; Fisher, A. C.; Wadhawan, J. D.; Cooper, J. J.; Ward, H. J.; Lawrence, N. S. A mechanistic study of the EC' mechanism—the split wave in cyclic voltammetry and square wave voltammetry. *RSC Adv.* **2016**, *6*, 70237–70242.
- (47) Evans, D. H. One-electron and two-electron transfers in electrochemistry and homogeneous solution reactions. *Chem. Rev.* **2008**, *108*, 2113–2144.
- (48) Datta, D. Two-step electron transfer & disproportionation of simple Cu<sup>+</sup> ion. *Indian J. Chem.* **1987**, *26A*, 605–606.
- (49) O'Sullivan, D. W.; Lee, M.; Noone, B. C.; Heikes, B. G. Henry's Law Constant Determinations for Hydrogen Peroxide, Methyl Hydroperoxide, Hydroxymethyl Hydroperoxide, Ethyl Hydroperoxide, and Peroxyacetic Acid. *J. Phys. Chem.* **1996**, *100*, 3241–3247.
- (50) Sander, R. Compilation of Henry's law constants (version 4.0) for water as solvent. *Atmos. Chem. Phys.* **2015**, *15*, 4399–4981.